STABILITY OF CLOSED LOOP FRACTIONAL ORDER SYSTEMS AND DEFINITION OF DAMPING CONTOURS FOR THE DESIGN OF CONTROLLERS

PATRICK LANUSSE* and ALAIN OUSTALOUP†
University of Bordeaux, IMS Laboratory – UMR 5218 CNRS,
Talence, 33405, France
**patrick.lanusse@ims-bordeaux.fr*
†*alain.oustaloup@ims-bordeaux.fr*

VALERIE POMMIER-BUDINGER
ISAE, DMIA Department,
Toulouse, 31055, France
valerie.budinger@isae.fr

Fractional complex order integrator has been used since 1991 for the design of robust control-systems. In the CRONE control methodology, it permits the parameterization of open loop transfer function which is optimized in a robustness context. Sets of fractional order integrators that lead to a given damping factor have also been used to build iso-damping contours on the Nichols plane. These iso-damping contours can also be used to optimize the third CRONE generation open loop transfer function. However, these contours have been built using nonband-limited integrators, even if such integrators reveal to lead to unstable closed loop systems. One objective of this paper is to show how the band-limitation modifies the left half-plane dominant poles of the closed loop system and removes the right half-plane ones. Also presented are how to obtain a fractional order open loop transfer function with a high phase slope and a useful frequency response, and how the damping contours can be used to design robust controllers, not only CRONE controllers but also PD and QFT controllers.

Keywords: Fractional order system; complex order integration; CRONE control; closed loop stability.

1. Introduction

The CRONE control-system design methodology has been developed since the 1980s [Oustaloup, 1983, 1991; Oustaloup & Mathieu, 1995b; Lanusse, 1994; Åström, 1999]. It is based on the common unity-feedback configuration (Fig. 1). The robust controller K or the open loop transfer function β is defined using fractional order integro-differentiation. The required robustness is that of both stability margins and performance, and particularly of resonant peak M_{T} of the complementary sensitivity function $T(s)$.

Three CRONE control design methods have been developed, successively extending the application field. If the CRONE method is devoted to the linear feedback system design using the controller as one Degree Of Freedom (DOF), it is obvious that a second DOF (linear or not) could be added outside the loop for managing pure tracking problems.

The variations of the phase margin (of a closed loop system) come both from the parametric variations of the plant G and from the controller phase variations around open loop gain crossover frequency ω_{cg}, which can also vary. The first

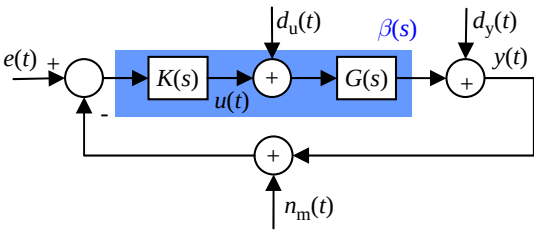

Fig. 1. Common CRONE control-system diagram.

generation CRONE control proposes a controller without phase variation (fractional differentiation) around ω_{cg}. Thus, phase margin variation only results from the plant variations. In order not to manage the accuracy of the closed loop control-system and in order to reduce the sensitivity of the control-system to high frequency measurement noise, the controller is defined from a band-limited fractional order differentiator. The rational approximation of this differentiator is achieved by using the well-known Oustaloup's frequency domain approximation method based on log-distributed zeros and poles [Oustaloup, 1983]. This strategy has to be used when ω_{cg} is within a frequency range where the plant phase is constant and also where the plant variations are only gain-like. Such a range is often in the high frequencies, and can lead to high-level control effort.

In second generation CRONE control, when the plant variations are gain-like around ω_{cg}, the plant phase variation, with respect to frequency, is cancelled by that of the controller. Thus, there is no phase margin variation when frequency ω_{cg} varies. Such a controller provides a constant open loop phase (real fractional order integration) whose Nichols locus is a vertical straight line called a frequency template. It revealed to be very close to the open loop frequency response proposed by Bode [1945]. This template ensures the robustness of phase and modulus margins and of resonant peaks of complementary sensitivity and sensitivity functions. The stability criterion proposed by Popov is commonly used to prove the stability of systems with interconnected memoryless nonlinearity and rational linear system. It has been shown how this criterion can be used to analyze the closed loop stability when the linear system is a fractional order integrator and when the nonlinear gain lies in a sector [Lanusse & Oustaloup, 2006]. Then, this gain has been interpreted as an unstructured uncertainty added to the structured uncertainty of the linear part of a plant model to design a second generation CRONE controller. In order to obtain an efficient controller, only a band-limited fractional order integrator is used at this step.

The third CRONE control generation must be used when the plant uncertainties are of various types (not only gain-like). The vertical template is then replaced by a generalized template always described as a straight line in the Nichols chart, but of any direction (complex fractional order integration) [Oustaloup, 1991; Lanusse *et al.*, 1992; Lanusse *et al.*, 1993; Lanusse, 1994]. An optimization allows the determination of the independent parameters of the nominal open loop transfer function. This optimization is based on the minimization of the stability degree variations, while respecting other specifications taken into account by constraints on sensitivity function magnitude. Iso-damping contours can be used to minimize the closed loop damping variations. The complex fractional order permits the parameterization of the open loop transfer function with a small number of high-level parameters. Thus, it makes easier the nonlinear optimization that needs to be used. Finally, the corresponding CRONE controller is synthesized as the rational transfer function that fits the desired frequency response the best. The third generation CRONE CSD methodology is able to design controllers for plants with right half-plane zeros or poles, time delay, and/or with lightly damped modes [Oustaloup *et al.*, 1995c; Pommier *et al.*, 2008]. Associated with the w-bilinear variable change, it also permits the design of digital controllers. The CRONE control has also been extended to linear time variant systems [Sabatier *et al.*, 2002] and nonlinear systems whose nonlinear behaviors are taken into account by sets of linear equivalent behaviors [Lanusse *et al.*, 1992; Pommier *et al.*, 2002, 2006]. For multivariable plants, two methods have been developed [Lanusse *et al.*, 1996, 2000; Pommier *et al.*, 2005; Nelson-Gruel *et al.*, 2008]. The choice of the method (multi-SISO, decentralized or fully MIMO) is made through an analysis of the coupling rate of the plant.

Even if they have been used for many years to design robust controllers and also to build a network of iso-damping contours around the -1 point of the Nichols chart, it is time to explain how the frequency band-limitation of fractional complex order integrators can modify the closed loop poles location and then how it ensures the closed loop

stability. Section 2 shows the properties of a system whose open loop transfer function is defined by a pure complex order integrator. Section 3 explains how the complex order integrator can be band-limited and how to obtain integrators whose order has a high imaginary part. Section 4 presents how the band-limitation of the integrator can modify the closed loop pole location. Section 5 shows how these contours can be used to design a simple PID robust controller. Then it is explained how the contours can be taken into account to design robust controllers using either the CRONE or QFT methodology.

2. Closed Loop Transfer Function Based on a Non-Band-Limited Complex Order Integrator

Even if the third generation of the CRONE methodology is based on an open loop transfer function defined by a non-band-limited complex order integrator around the gain crossover frequency ω_{cg}

$$\beta(s) = \left(\cosh\left(b\frac{\pi}{2}\right)\right)^{\mathrm{sign}(b)} \left(\frac{\omega_{\mathrm{cg}}}{s}\right)^{a} \times \frac{\mathrm{Re}}{i}\left(\left(\frac{\omega_{\mathrm{cg}}}{s}\right)^{ib}\right)^{-\mathrm{sign}(b)}, \qquad (1)$$

using the Nyquist stability criterion, it is simple to show that without any band-limitation, the closed loop which would be obtained would be unstable when $b \neq 0$. Re/i means that only the real part with respect to the imaginary number i (in the integration complex order) is taken into account. The i number is not to be confused with the imaginary number j that is used in the s Laplace variable. i is a genuine imaginary number without any physical meaning whereas j is used to model a dynamic behavior.

Proof. Oustaloup *et al.* [2000] showed that a complex order differentiator can be approximated by an infinite number of left half-plane complex zeros and poles. The two complex recursive factors that characterize the distribution are functions of the complex fractional order of the differentiator. As an infinite number of zeros and poles is used, the modulus of the two recursive factors tend to 1 from above. Thus, each fractional order part of the open loop transfer function (1) can also be approximated by left half-plane zeros and poles only, that is to say without any right half-plane pole.

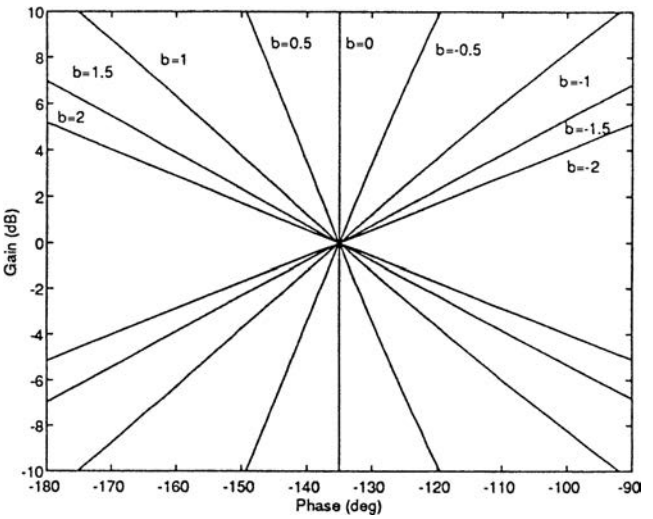

Fig. 2. Nichols diagram of $\beta(\mathrm{j}\omega)$ for a given real integration order $a = 1.5$ and various imaginary integration orders.

The magnitude and phase of β defined by (1) are:

$$|\beta(\mathrm{j}\omega)| = \left(\cosh\left(b\frac{\pi}{2}\right)\right)^{\mathrm{sign}(b)} \left(\frac{\omega_{\mathrm{cg}}}{\omega}\right)^{a} \times \left(\cos^2\left(b\ln\left(\frac{\omega_{\mathrm{cg}}}{\omega}\right)\right) + \sinh^2\left(b\frac{\pi}{2}\right)\right)^{-\frac{\mathrm{sign}(b)}{2}}$$

$$\arg\beta(\mathrm{j}\omega) = -a\frac{\pi}{2} - \mathrm{sign}(b) \times \mathrm{atan}\left[\tan\left(b\ln\left(\frac{\omega_{\mathrm{cg}}}{\omega}\right)\right)\tanh\left(b\frac{\pi}{2}\right)\right]. \qquad (2)$$

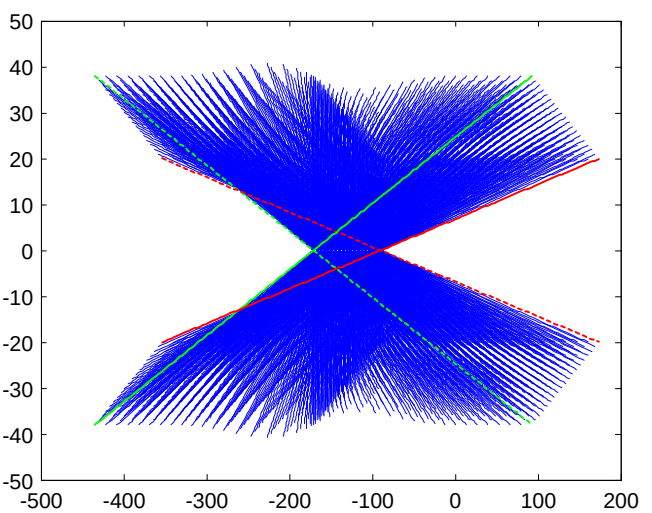

Fig. 3. Nichols diagram of $\beta(\mathrm{j}\omega)$ for a between 1 (red) and 1.9 (green) and b between -2 (solid) and 2 (dash).

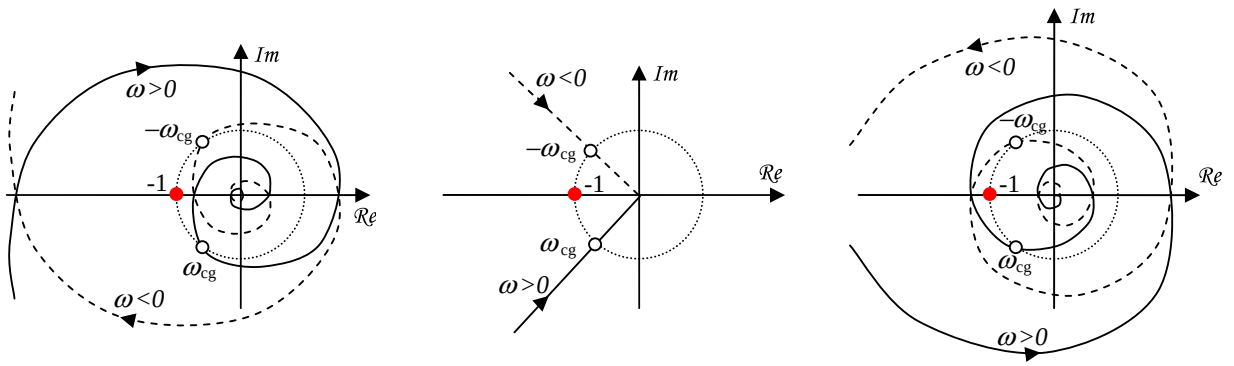

(a) (b) (c)

Fig. 4. Nyquist diagrams of $\beta(\mathrm{j}\omega)$ for $a = 1.5$ and: (a) negative b, (b) null b and (c) positive b.

Then for $\omega = \omega_{\mathrm{cg}}$:

$$|\beta(\mathrm{j}\omega)| = 1; \quad \arg\beta(\mathrm{j}\omega) = -a\frac{\pi}{2};$$

$$\frac{\partial|\beta(\mathrm{j}\omega)|_{\mathrm{dB}}}{\partial\log_{10}\omega} = -20a \quad \text{and} \tag{3}$$

$$\frac{\partial\arg(\beta(\mathrm{j}\omega))}{\partial\log_{10}\omega} = \ln(10)\mathrm{sign}(b)b\tanh\left(b\frac{\pi}{2}\right).$$

Figure 2 presents the Nichols diagram of $\beta(\mathrm{j}\omega)$ for $a = 1.5$ and various values of the imaginary integration order.

Then, Fig. 3 shows the Nichols diagram of $\beta(\mathrm{j}\omega)$ computed for a set of values of a between 1 and 1.9 (with increments of 0.05), for a set of values of b between -2 and 2 (with increments of 0.1) and for $\omega_{\mathrm{cg}} = 1$. Figures 4(a)–4(c) show the shape of the Nyquist diagram of $\beta(\mathrm{j}\omega)$ for $a = 1.5$ and respectively for negative, null and positive values of b.

As the phase of $\beta(\mathrm{j}\omega)$ goes from $+\infty$ to $-\infty$ for negative b [Fig. 4(a)], $\beta(\mathrm{j}\omega)$ reveals an infinite number of counter clockwise encirclements of -1 critical point. As the phase of $\beta(\mathrm{j}\omega)$ goes from $-\infty$ to $+\infty$ for positive b [Fig. 4(c)], $\beta(\mathrm{j}\omega)$ reveals an infinite number of counter clockwise encirclements of -1. Only for null b [Fig. 4(b)], $\beta(\mathrm{j}\omega)$ does not encircle -1.

Thus, as there is no right half-plane pole in the open loop transfer function $\beta(s)$ whatever the value of b, the Nyquist stability criterion shows that the closed loop system is only stable for null b. ■

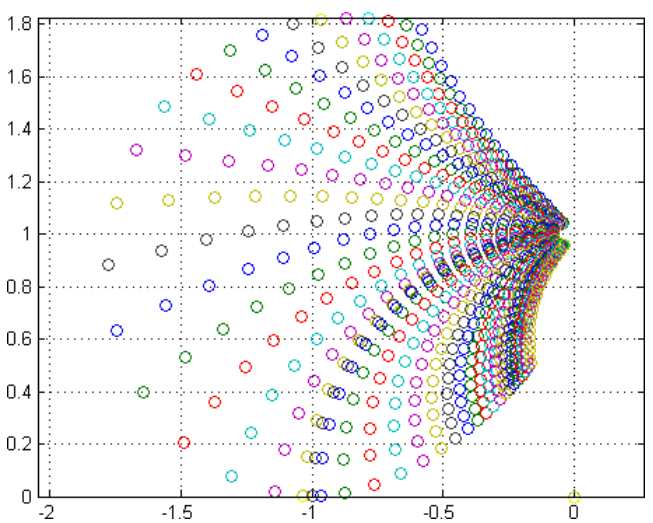

Fig. 5. Loci of the left half-plane pole of $\beta(s)/(1+\beta(s))$ with a positive imaginary part for a between 1 and 1.9, b between -2 and 2 and $\omega_{\mathrm{cg}} = 1$.

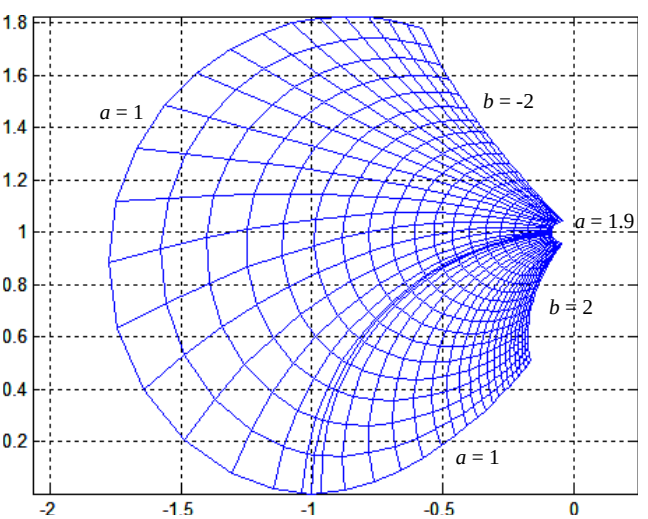

Fig. 6. Iso-a and iso-b loci of the stable upper pole of $\beta(s)/(1+\beta(s))$ for a between 1 and 1.9 (with increments of 0.05), b between -2 and 2 (with increments of 0.1) and $\omega_{\mathrm{cg}} = 1$.

Even if the closed loop transfer function $\beta(s)/(1+\beta(s))$ includes right half-plane poles, it also includes one left half-plane complex conjugated pole pair. The stable roots of $\beta(s)+1=0$ had been used to build iso-damping contours [Lanusse, 1994; Oustaloup *et al.*, 1995a, 2003]. Figure 5 shows how the left half-plane closed loop pole (numerically found) with the positive imaginary part moves when a and b vary.

Figure 6 presents the "shell" that builds this stable pole when either a or b varies.

3. Closed Loop Transfer Function Based on a Band-Limited Complex Order Integrator

In order to ensure the stability of the closed loop system, and thus to ensure that the used poles are the genuine dominant poles that govern the time-domain response, the imaginary order part of the integrator needs to be band-limited. Thus definition (1) of $\beta(s)$ can be replaced by:

$$\beta(s)=K\left(\frac{\omega_{\rm cg}}{s}\right)^a \frac{\mathrm{Re}}{i}\left(\left(\alpha_0\frac{1+\dfrac{\omega_{\rm h}}{s}}{1+\dfrac{\omega_{\rm l}}{s}}\right)^{ib_q}\right)^{-q\,\mathrm{sign}(b_q)}, \tag{4}$$

where K ensures that $|\beta(\mathrm{j}\omega_{\rm cg})|=1$, $\alpha_0=\sqrt{\frac{\omega_{\rm cg}^2+\omega_{\rm l}^2}{\omega_{\rm cg}^2+\omega_{\rm h}^2}}$ and q is a positive integer number.

Figure 7 shows how the band-limitation modifies the Nichols locus of $\beta(s)$.

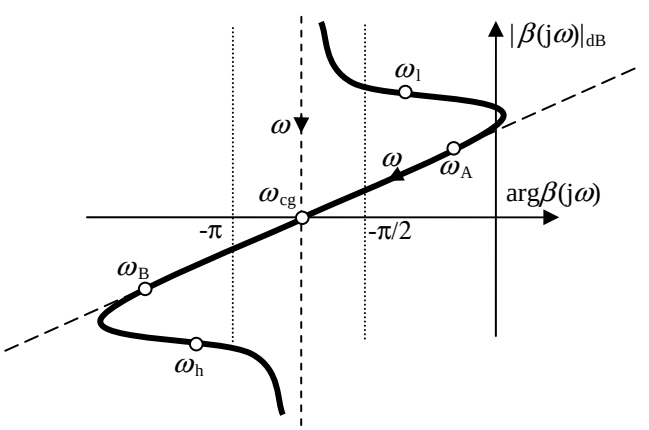

Fig. 7. Nichols diagrams of $\beta(\mathrm{j}\omega)$ for $a=1.5$ and: null b_q (- -); negative b_q and β defined by (4) (——); negative b_q and β defined by (1) (– –).

Figure 7 shows that the open loop frequency response with the band-limited integrator looks like the initial open loop frequency response on a frequency range $[\omega_{\rm A},\omega_{\rm B}]$, shorter more narrow than the frequency range $[\omega_{\rm l},\omega_{\rm h}]$.

When ω tends to 0 and $+\infty$, it has been shown (already used in [Lanusse, 1994]) that the phase of $\beta(\mathrm{j}\omega)$ tends to $a\pi/2$ if and only if:

$$|b_q|<\min\left(\frac{\pi}{2\ln(\alpha_0)},\frac{\pi}{2\left|\ln\left(\alpha_0\dfrac{\omega_{\rm l}}{\omega_{\rm h}}\right)\right|}\right). \tag{5}$$

For $\omega=\omega_{\rm cg}$, the slope of the phase of $\beta(\mathrm{j}\omega)$ is now given by:

$$\frac{\partial\arg(\beta(\mathrm{j}\omega))}{\partial\log_{10}\omega}=\gamma\ln(10)q\,\mathrm{sign}(b_q)b_q\tanh(b_q(\theta_{\rm h}-\theta_{\rm l})) \tag{6}$$

where

$$\gamma=\omega_{\rm cg}^2\left(\frac{1}{\omega_{\rm cg}^2+\omega_{\rm h}^2}-\frac{1}{\omega_{\rm cg}^2+\omega_{\rm l}^2}\right)\quad\text{and}$$

$$\theta_{\rm l,h}=\mathrm{atan}\left(\frac{\omega_{\rm cg}}{\omega_{\rm l,h}}\right).$$

For $b_q=b$ and $q=1$, it is easy to verify that (6) tends to its value in (3) when $\omega_{\rm l}$ tends to 0 and when $\omega_{\rm h}$ tends to ∞.

For given values of $\omega_{\rm cg}$, $\omega_{\rm l}$ and $\omega_{\rm h}$, and for a desired value of the slope of the phase (related to a given initial value of b), q is defined as the smallest integer number that leads to a value of b_q that meets (5) and is the solution of the nonlinear equation:

$$q\mathrm{sign}(b_q)b_q\tanh(b_q(\theta_{\rm h}-\theta_l))=\mathrm{sign}(b)b\tanh(b(\theta_{\rm h}-\theta_l)). \tag{7}$$

For large values of $\tanh(b(\theta_h-\theta_l))$, b_q is very close to b/q.

4. Pole Location of a Closed Loop System Defined From a Band-Limited Complex Order Integrator

The risk of closed loop instability is reduced when the band-limitation is managed with a reduced $\omega_{\rm h}/\omega_{\rm l}$ ratio. When this ratio is close to 1, α_0 in (5) is also close to 1 and thus the limit value of b_q is very large. Figure 8 shows the Nichols diagram of

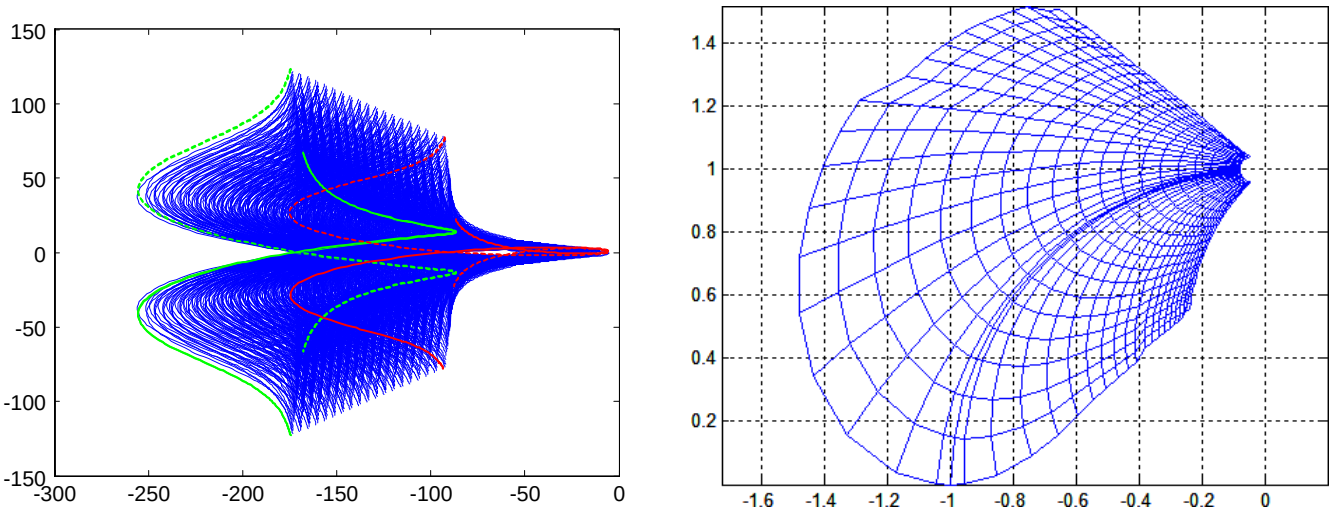

(a) (b)

Fig. 8. For $\omega_{\rm h}/\omega_{\rm l} = 10$: (a) Nichols diagram of $\beta(\mathrm{j}\omega)$ for a between 1 (red) and 1.9 (green), b between -2 (solid) and 2 (dash); (b) iso-a and iso-b loci of the stable upper pole of $\beta(s)/(1+\beta(s))$.

$\beta(\mathrm{j}\omega)$ defined by (4) and obtained for several values of a between 1 and 1.9 (with increments of 0.05), several values of b between -2 and 2 (with increments of 0.1), and for $\omega_{\rm cg} = 1$, $\omega_l = 1/10^{0.5}$ and $\omega_{\rm h} = 10^{0.5}$.

Figure 8(a) shows now that the phase of all the frequency responses tends to $-a\pi/2$ when ω tends to $\pm\infty$. As above, the poles of $\beta(s)/(1+\beta(s))$ are searched. Now there is only one left half-plane conjugated complex pair pole (no right half-plane pole) and one of them is plotted [Fig. 8(b)]. As the band-limitation reduces the linearity of the Nichols diagram of $\beta(\mathrm{j}\omega)$ around the critical point, the deformed shell obtained would not provide the iso-damping contours proposed in [Lanusse, 1994] and used in [Oustaloup *et al.*, 2003].

Figure 9(a) shows the Nichols diagram of $\beta(\mathrm{j}\omega)$ obtained now for $\omega_l = 0.1$ and $\omega_{\rm h} = 10$. As the $\omega_{\rm h}/\omega_{\rm l}$ ratio increases, for a same phase slope (related to the value of b between -2 and 2), the integer number q needs to increase in order that b_q meets (5). When the phase of these frequency

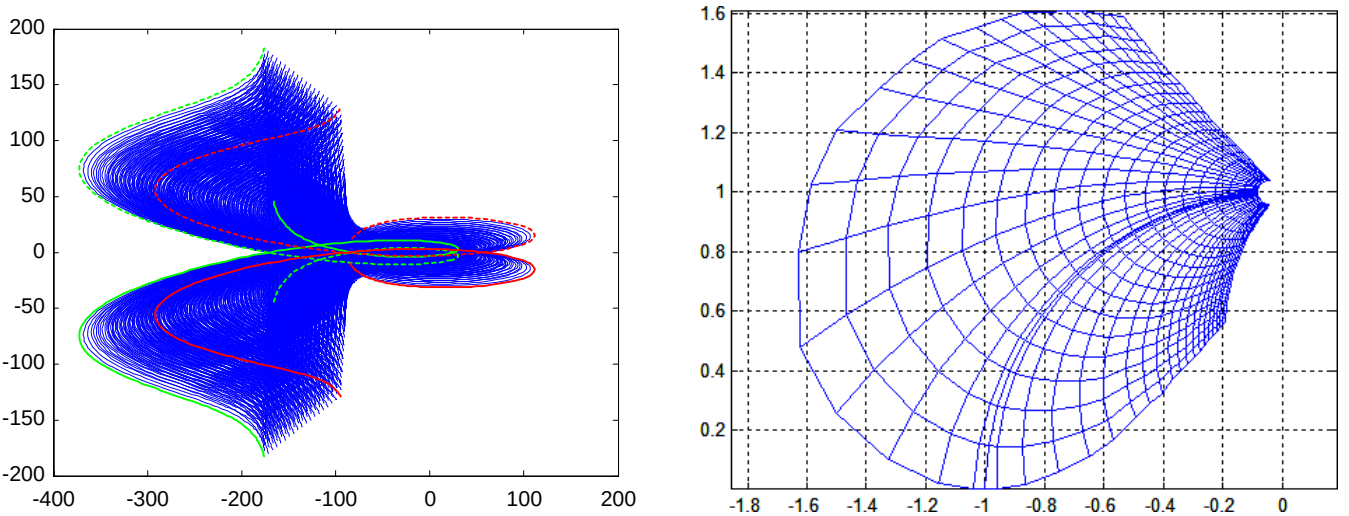

(a) (b)

Fig. 9. For $\omega_{\rm h}/\omega_{\rm l} = 10^2$: (a) Nichols diagram of $\beta(\mathrm{j}\omega)$ for a between 1 (red) and 1.9 (green), b between -2 (solid) and 2 (dash); (b) iso-a and iso-b loci of the stable upper pole of $\beta(s)/(1+\beta(s))$.

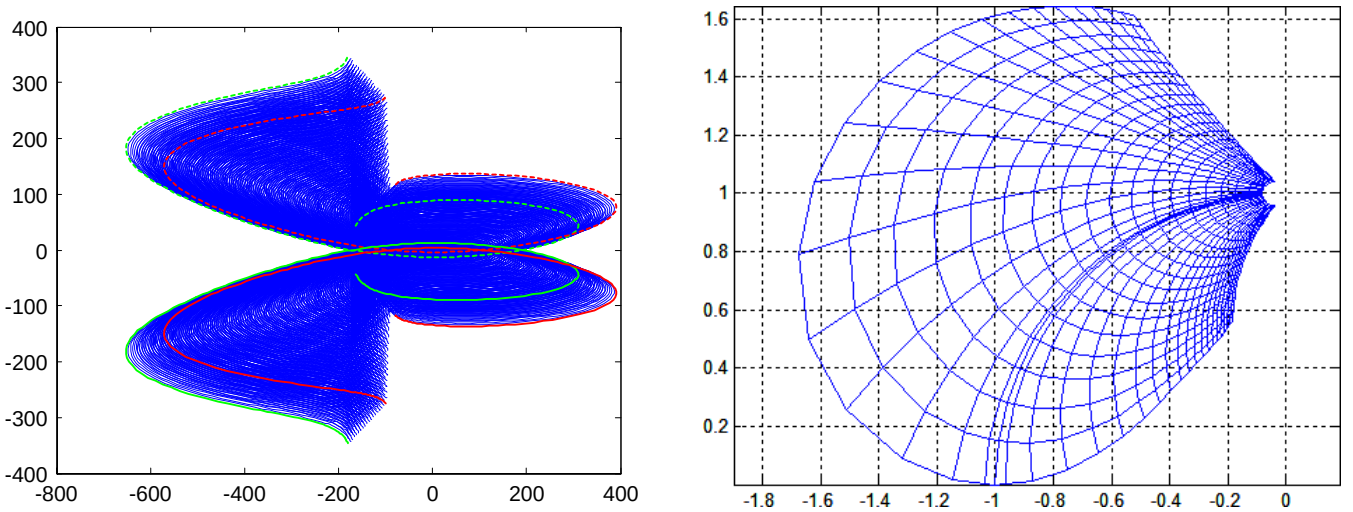

(a) (b)

Fig. 10. For $\omega_h/\omega_l = 10^4$: (a) Nichols diagram of $\beta(j\omega)$ for a between 1 (red) and 1.9 (green), b between -2 (solid) and 2 (dash); (b) iso-a and iso-b loci of the stable upper pole of $\beta(s)/(1+\beta(s))$.

responses becomes positive, Fig. 9(a) shows that the gain increases (also for frequencies greater than ω_{cg}). Figure 9(b) presents the loci of the upper pole of $\beta(s)/(1+\beta(s))$. Even, if the difference is weaker than before, this new shell remains different from the shell of Fig. 6 used to build the iso-damping contour.

Finally, the open loop transfer function β is computed with $\omega_h/\omega_l = 10^4$. Figures 10(a) and 10(b) show respectively the open loop frequency responses and the closed loop poles. It can be concluded that when the frequency band $[\omega_l, \omega_h]$ increases and when the closed loop stability is ensured by using the power parameter q and the order b_q of (4), the closed loop poles tends to the closed loop left half-plane poles pair related to b and (1).

Thus, the shell presented by Fig. 6 can really be used to build iso-damping contours (Fig. 11), each contour being defined as the envelope of all the open loop frequencies leading to a same closed loop damping ratio value ζ (that is, for a same closed loop pole argument). From these contours and using interpolation methods, it is possible to define approximative iso-damping contours. A polynomial function is used to draw the contour C_ζ for ζ between 0.1 and 0.9:

$$C_\varsigma : X^\circ = \sum_{j=0}^{2} f_j(\varsigma) Y_{\mathrm{dB}}^{2j} \quad \text{with } f_j(\varsigma) = \sum_{k=0}^{3} a_{jk}\varsigma^k, \tag{8}$$

where X and Y are the Nichols-plane coordinates of a point of C_ζ. The coefficients a_{jk} are given in Table 1.

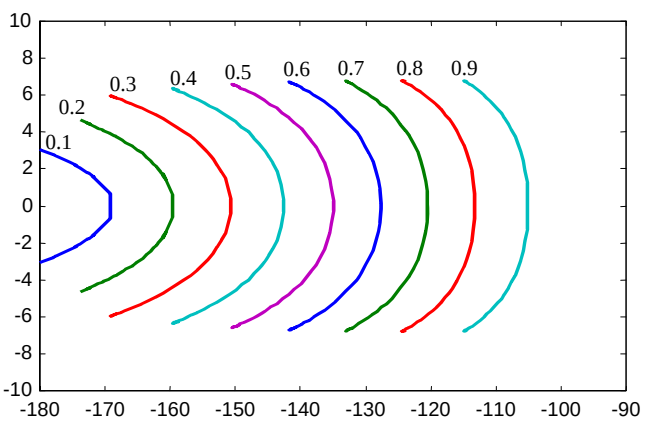

Fig. 11. Set of iso-damping contours on the Nichols plane for ζ between 0.1 and 0.9 (with 0.1 increments).

Table 1. Values of coefficients a_{jk}.

		k			
		0	1	2	3
j	0	−180.36	117.70	−74.316	40.376
	1	−1.1538	3.8888	−5.2999	2.5417
	2	−0.0057101	0.0080962	−0.0060354	0.0016158

5. Design of Controllers Using Damping Contours

5.1. *Design of a robust PID controller*

Let the transfer function of a perturbed plant be:

$$G(s) = \frac{k}{s\left(1 + \dfrac{s}{\omega_c}\right)}$$

$$\text{with } k \in [0.5, 2] \text{ and } \omega_c \in [0.5, 2]. \quad (9)$$

For the nominal parametric state of the plant, the parameters are $k_0 = 1$ and $\omega_{c0} = 1$. Using a PID controller, our first objective is to ensure a closed loop pole damping ratio greater than 0.5 for all the possible parametric states of the plant. The controller is defined by:

$$K(s) = K_0 \frac{1+s}{s} \frac{1 + \dfrac{as}{\omega_m}}{1 + \dfrac{s}{a\omega_m}}. \quad (10)$$

The other objectives are: the nominal open loop gain crossover frequency equals 1 rad/s; a lead effect as small as possible (the smallest value of a). Parameters K_0, a and ω_m which ensure tangency to the 0.5 iso-damping contour are $K_0 = 0.25$, $a = 3.5$ and $\omega_m = 0.85$. Figure 12 shows a set of 25 possible open loop Nichols loci and the tangencies both to the specified 0.5 iso-damping ratio and to a 3.34 dB Nichols magnitude contour. Using the relationship between resonant peak M_T and damping ratio ζ,

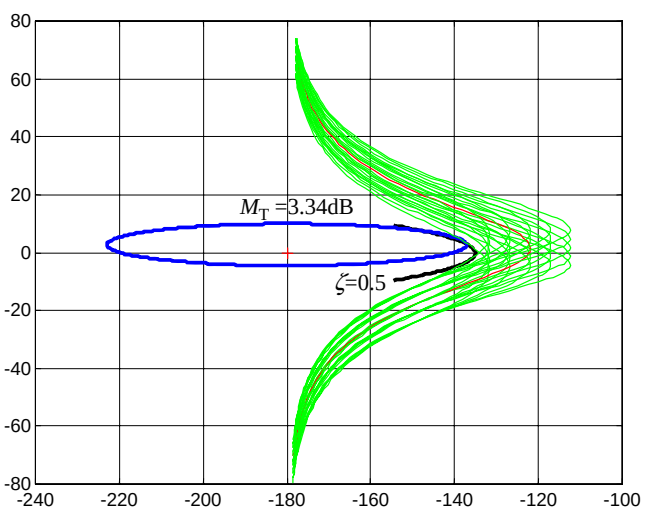

Fig. 12. Open loop Nichols loci, 0.5 iso-damping and 3.34 dB magnitude contours (nominal in red).

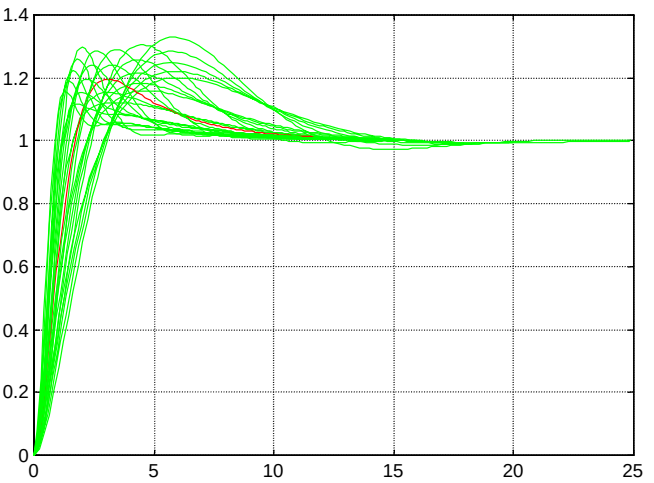

(a)

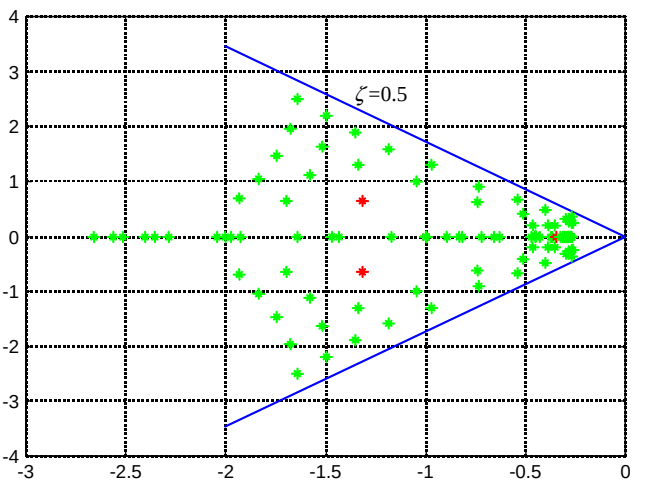

(b)

Fig. 13. (a) Closed loop step responses, (b) poles and 0.5 damping ratio limit. Nominal in red, perturbed in green.

defined for second order systems, this resonant peak value would predict a 0.36 damping ratio. Figure 13(a) gives the corresponding closed loop step responses.

Figure 13(b) shows the location of the closed loop-poles. From these poles, the actual smallest value of closed loop-pole damping ratios is 0.54. This example shows that the damping ratio predicted in the frequency domain using iso-damping contours (0.5) is much closer to its actual value (0.54) than when using common magnitude contours (0.36). It is thus demonstrated that these iso-damping contours can be used in frequency-based design for angular placement of closed loop poles. Finally, this example shows that iso-damping

contours can also be used when the open loop locus is not rectilinear but close to a rectilinear locus near the resonant frequency.

5.2. *Robust control design using the CRONE control methodology*

The third generation CRONE control methodology is also able to use iso-damping contours [Pommier *et al.*, 2008]. Its principle is to optimize the parameter of a nominal open loop transfer function that includes a band-limited complex fractional order integration:

$$\beta(s) = \beta_{\rm l}(s)\beta_{\rm m}(s)\beta_{\rm h}(s), \tag{11}$$

where $\beta_{\rm m}(s)$ is a set of band-limited generalized templates:

$$\beta_{\rm m}(s) = \prod_{k=-N^-}^{N^+} \beta_k(s), \tag{12}$$

with

$$\beta_k(s) = C_k^{\mathrm{sign}(b_k)} \left(\alpha_k \frac{1+\dfrac{s}{\omega_{k+1}}}{1+\dfrac{s}{\omega_k}} \right)^{a_k} \times \left(\frac{\Re e}{\mathrm{i}} \left\{ \left(\alpha_k \frac{1+\dfrac{s}{\omega_{k+1}}}{1+\dfrac{s}{\omega_k}} \right)^{\mathrm{i}b_k} \right\} \right)^{-q_k \mathrm{sign}(b_k)} \tag{13}$$

and

$$\alpha_k = \left(\frac{\omega_{k+1}}{\omega_k} \right)^{1/2} \quad \text{for } k \neq 0 \quad \text{and}$$
$$\alpha_0 = \left(\frac{1+\left(\dfrac{\omega_{\rm r}}{\omega_0}\right)^2}{1+\left(\dfrac{\omega_{\rm r}}{\omega_1}\right)^2} \right)^{1/2} \tag{14}$$

where $\beta_l(s)$ is an integer order $n_{\rm l}$ proportional integrator and where $\beta_{\rm h}(s)$ is a low-pass filter of integer order $n_{\rm h}$:

$$\beta_{\rm l}(s) = C_{\rm l} \left(\frac{\omega_{-N^-}}{s} + 1 \right)^{n_{\rm l}},$$
$$\beta_{\rm h}(s) = C_{\rm h} \left(\frac{s}{\omega_{N^+}} + 1 \right)^{-n_{\rm h}}. \tag{15}$$

Gains C_x (C_k, $C_{\rm l}$ and $C_{\rm h}$) are such that $\omega_{\rm r}$ is the closed loop resonant frequency. Order $n_{\rm l}$ has to be set to manage the accuracy provided by the control-system. Order $n_{\rm h}$ has to be set to obtain a proper or bi-proper controller. When it is useful, N^- and N^+ are different from 0 to increase the number of tuning parameters.

Even if the open loop parameters are often optimized in order to reduce the variation of the resonant peak $M_{\rm T}$, the optimal open loop transfer function can also be obtained by the minimization of one of the following robustness cost functions:

- $J = \zeta_0 - \inf_G |\zeta|,$ (16)
- $J = \left(\zeta_0 - \inf_G |\zeta| \right)^2 + \left(\sup_G |\zeta| - \zeta_0 \right)^2,$ (17)
- $J = \sup_G |\zeta| - \inf_G |\zeta|,$ (18)

where ζ_0 is a required value of the nominal closed loop damping ratio (for the nominal plant G_0), while respecting the following set of inequality constraints for all plants G and for $\omega \in \mathbb{R}^+$:

$$\inf_G |T(\mathrm{j}\omega)| \geq T_{\rm l}(\omega), \quad \sup_G |T(\mathrm{j}\omega)| \leq T_{\rm u}(\omega),$$
$$\sup_G |S(\mathrm{j}\omega)| \leq S_{\rm u}(\omega), \quad \sup_G |KS(\mathrm{j}\omega)| \leq KS_{\rm u}(\omega)$$
$$\text{and} \quad \sup_G |GS(\mathrm{j}\omega)| \leq GS_{\rm u}(\omega), \tag{19}$$

with

$$\begin{cases} T(s) = \dfrac{K(s)G(s)}{1+K(s)G(s)} \\ S(s) = \dfrac{1}{1+K(s)G(s)} \\ KS(s) = \dfrac{K(s)}{1+K(s)G(s)} \\ GS(s) = \dfrac{G(s)}{1+K(s)G(s)} \end{cases}. \tag{20}$$

As the uncertainties are taken into account by the least conservative method, a nonlinear optimization method must be used to find the optimal values. For $N^- = N^+ = 0$, only four independent parameters have to be optimized. The parameterization of the open loop transfer function by complex

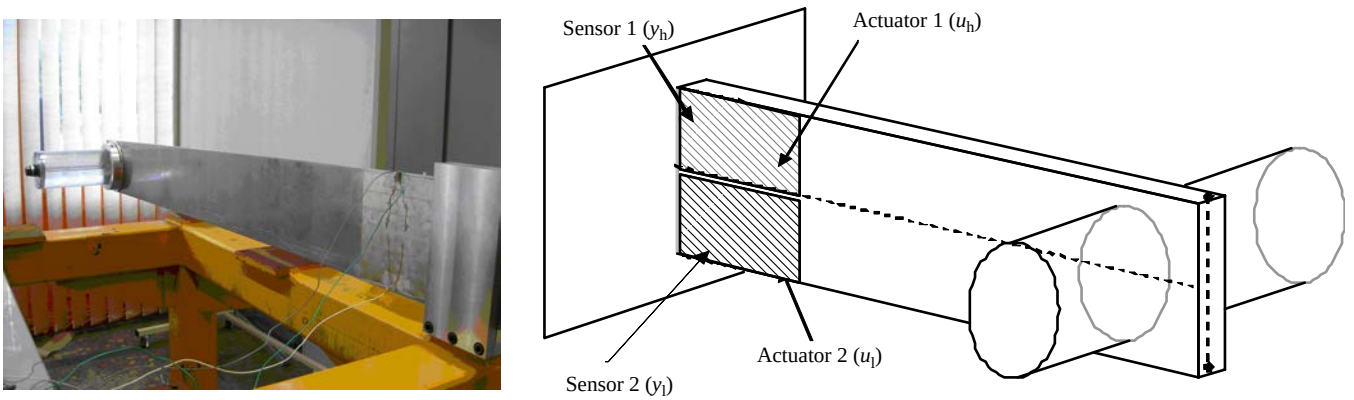

Fig. 14. Beam and tank system with piezoelectric sensors and actuators.

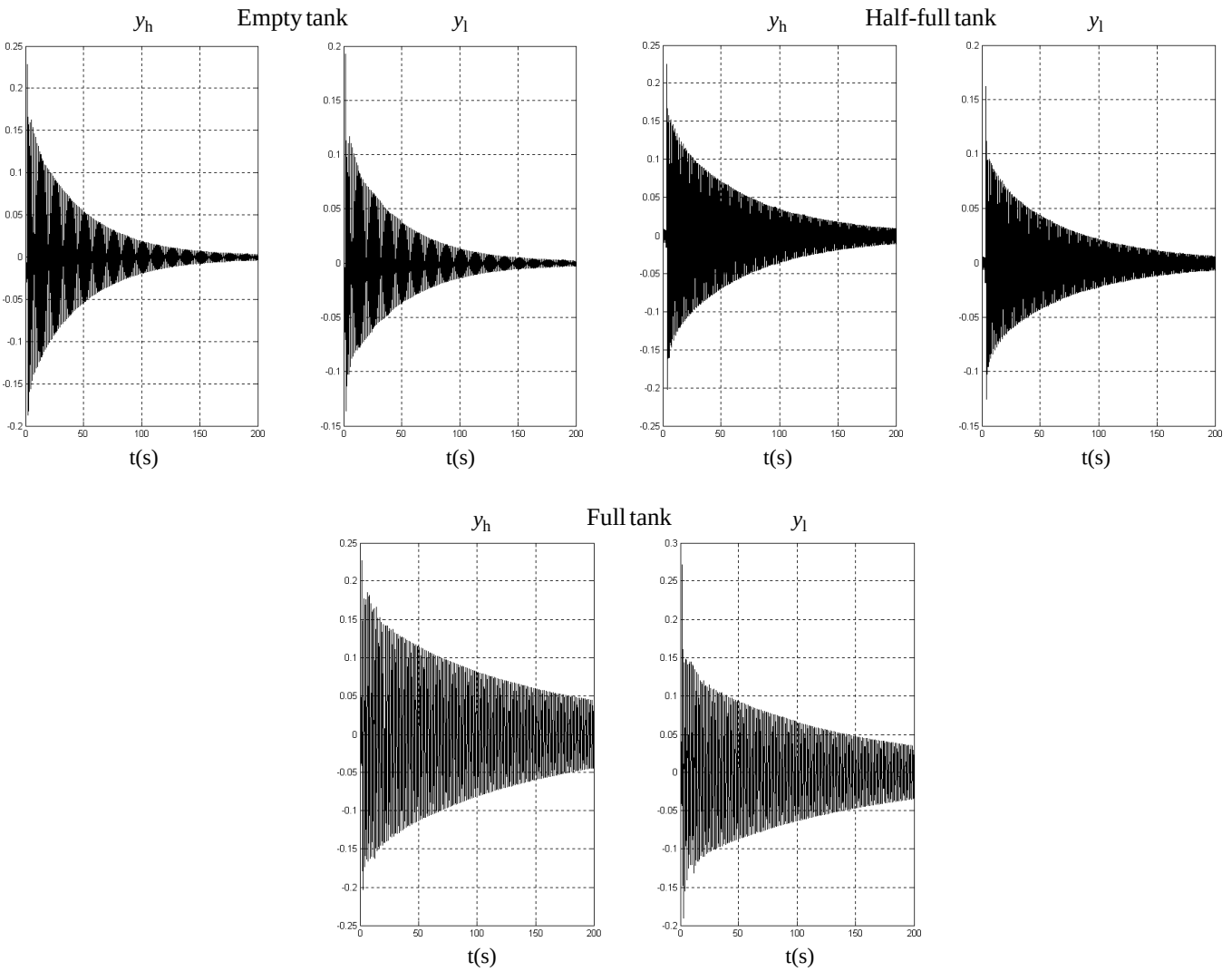

Fig. 15. Open loop time responses for three filling levels of the tank.

fractional orders, then simplifies the optimization considerably. During optimization a complex order has the same function as a whole set of parameters found in common rational controllers. Finally, the fractional controller $K_F(s)$ is defined by its frequency response:

$$K_{\mathrm{F}}(\mathrm{j}\omega) = \frac{\beta(\mathrm{j}\omega)}{G_0(\mathrm{j}\omega)}, \tag{21}$$

where $G_0(\mathrm{j}\omega)$ is the nominal frequency response of the plant. The parameters of a rational transfer function $K_{\mathrm{R}}(s)$ with a predefined low order structure are tuned to fit the ideal frequency response $K_{\mathrm{F}}(j\omega)$. Any frequency-domain system identification technique can be used. An advantage of this design method is that whatever the complexity of the control problem, low values of the controller order can be used (usually around 6).

The CRONE control methodology has been extended to MIMO systems [Nelson-Gruel *et al.*, 2009]. Its main principle is to optimize the parameters of a nominal and diagonal open loop transfer function matrix whose diagonal elements are defined by (11). It can be used to control a beam and tank system (Fig. 14) that models an aircraft wing. This system exhibits extremely low-damped vibrations that depend on the level of filling of the tank (Fig. 15). About 200 sec was required to obtain damped vibrations. These vibrations are measured by two piezoelectric ceramics (y_{l} and y_{h}). Two other piezoelectric ceramics (u_{l} and u_{h}) will be used as actuators to improve this damping.

Each open loop nominal and diagonal element ensures a gain cross-over frequency equal to 3 rad/s, a closed loop damping ratio ζ greater than $\zeta_0 = 0.1$ and a maximum of the sensitivity function KS lower than 50 dB. It is also defined by a low frequency order $n_{\mathrm{l}} = -1$ in order to limit the gain of the controllers in low frequencies and a high frequency order $n_{\mathrm{h}} = 4$ in order to limit the amplification of the noise. For the first open loop element $\beta_{01}(\mathrm{s})$, the optimized parameters are defined by $a_0 = 0.0037$, $b_{q0} = 3.05$, $q_0 = 5$, $\omega_0 = 1.4$ rad/s and $\omega_1 = 3.3$ rad/s. For the second open loop element $\beta_{02}(\mathrm{s})$, the optimal parameters are $a_0 = 2.99$, $b_{q0} = 1.81$, $q_0 = 5$, $\omega_0 = 1.3$ rad/s and $\omega_1 = 3.3$ rad/s. Figure 16 shows the Nichols loci with the uncertainty domains of the optimal open loop frequency responses computed from the diagonal elements of the closed loop complementary sensitivity function $T(s) = (I + G(s)K(s))^{-1}G(s)K(s)$.

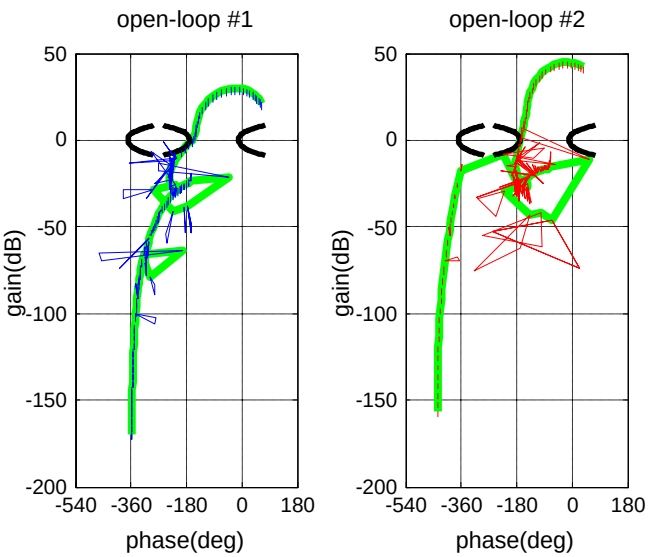

Fig. 16. Open loop frequency response (nominal in green) and 0.1 damping ratio limit (black).

The matrix of the controller is computed from the relation:

$$\begin{aligned} K(s) &= \begin{bmatrix} K_{11}(s) & K_{12}(s) \\ K_{21}(s) & K_{22}(s) \end{bmatrix} \\ &= \begin{bmatrix} G_{11_0}(s) & G_{12_0}(s) \\ G_{21_0}(s) & G_{22_0}(s) \end{bmatrix}^{-1} \begin{bmatrix} \beta_{11_0}(s) & 0 \\ 0 & \beta_{22_0}(s) \end{bmatrix}. \end{aligned} \tag{22}$$

The four terms of this matrix are synthesized by frequency domain system identification. Figure 17 shows how this robust controller is efficient to improve the damping. Now, the vibrations disappear before 25 sec.

5.3. *How to use iso-overshoot and iso-damping contours with QFT design*

QFT (Quantitative Feedback Theory) is a frequency-based method developed by Horowitz to design robust controllers [Horowitz *et al.*, 1972; Horowitz, 1991, 1993; D'Azzo & Houpis, 1995]. When using the QFT technique [Banos *et al.*, 2008; Cervera & Houpis, 2008] complex fractional order transfer functions were also used to design controllers with the QFT technique, the time requirements need to be translated into closed loop frequency bounds, and then into open loop boundaries constructed on the Nichols chart.

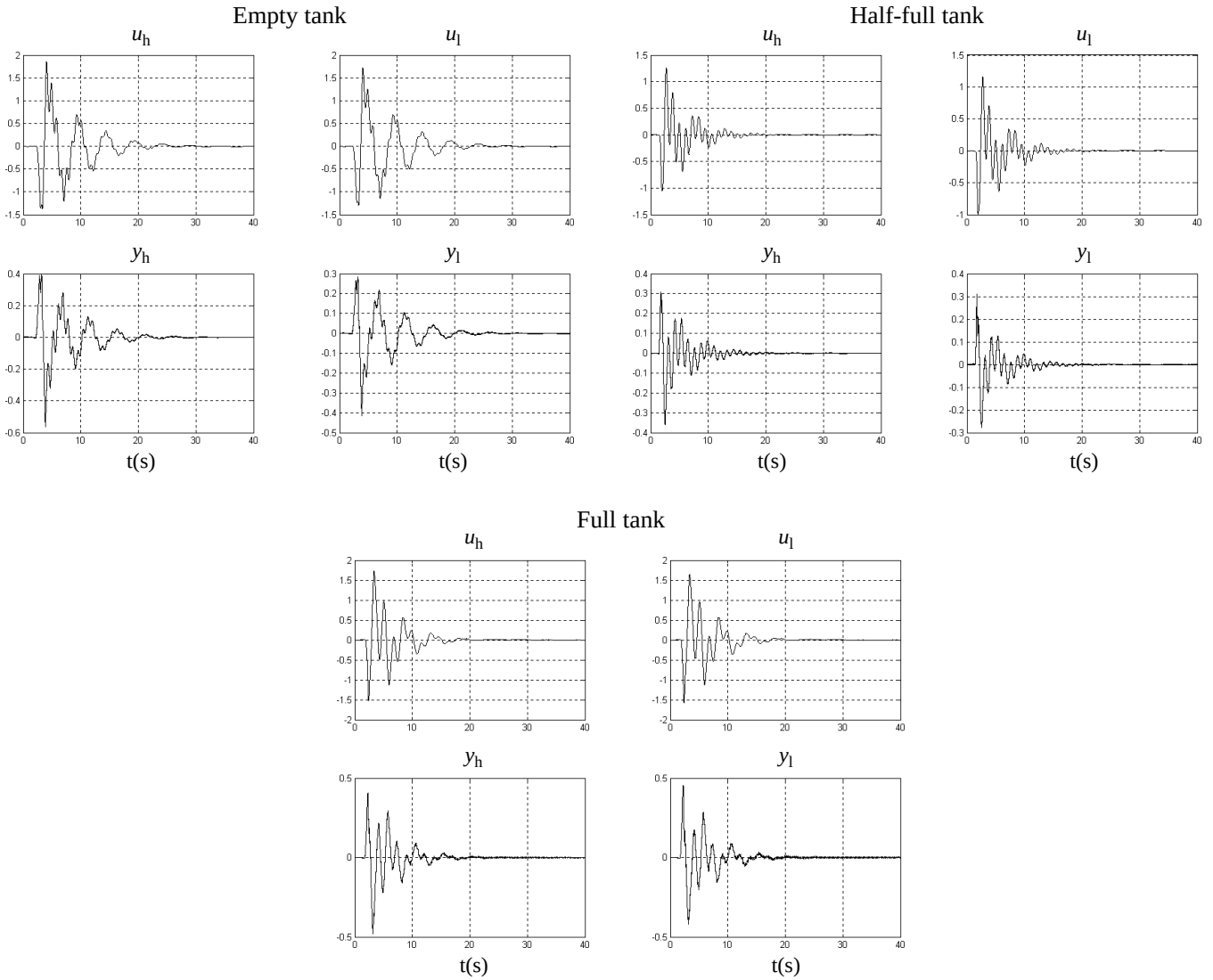

Fig. 17. Closed loop time responses for three filling levels of the tank.

The peak magnitude M_T of $T(s)$ is known to be strongly correlated to the step response overshoot, and the magnitude contours are used by frequency-based control-system designs. So limiting the upper value of the overshoot is obtained through avoiding penetration by the open loop Nichols locus of the area within the corresponding M_{Tu} magnitude contour of the Nichols chart. As QFT design deals with uncertain systems, the limitation of the step response overshoot for a set of plant models, is obtained using a set of boundaries $\{B_{Tu}(\omega_i)\}$ constructed from the M_{Tu} magnitude contour and from the set of plant frequency-response uncertainty domains $\{D(\omega_i)\}$ (called *template* in QFT terminology) computed for a set of well-chosen frequencies $\{\omega_i\}$. For a given frequency ω_i, the boundary $B_{Tu}(\omega_i)$ is constructed to ensure that the uncertain open loop frequency responses $\beta(j\omega_i)$ (described by its nominal value plus $\{D(\omega_i)\}$) do not penetrate the area of $B_{Tu}(\omega_i)$ when the arbitrary nominal open loop frequency response $\beta_0(j\omega_i)$ does not.

Figure 18 shows how boundaries can be constructed. The black dot of uncertainty domain $D(\omega_i)$ locates the nominal point corresponding to a nominal plant $G_0(s)$. The boundary is the locus drawn by the nominal point when $D(\omega_i)$ moves around and tangents the M_{Tu} magnitude contour. Thus the black dots are the "vertices" of $B_{Tu}(\omega_i)$. Figure 18(a) shows the construction for a polygonal uncertainty domain. Figure 18(b) shows the construction for a rectilinear uncertainty domain resulting from a plant where only a gain is

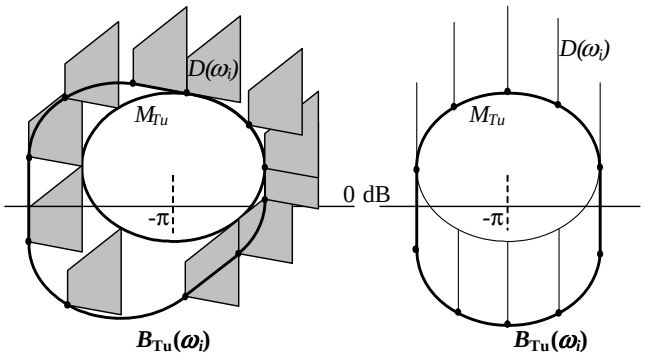

(a) (b)

Fig. 18. Construction of B_{Tu} boundaries of QFT designs for two types of uncertainty domains $D(\omega_i)$: (a) polygonal; (b) rectilinear.

uncertain. In this case the boundary is a U-contour as described by D'Azzo and Houpis [1995].

What is commonly done using magnitude contours to limit the upper value of the step response overshoot, can also be done using iso-damping contours to limit the lower value of the closed loop damping ratio at ζ_{l}. Figure 19 shows that the construction method of the boundary $B_{\zeta\mathrm{l}}(\omega_i)$ is similar to that of $B_{\mathrm{Tu}}(\omega_i)$: the M_{Tu} magnitude contour is only replaced by the iso-damping contour $C_{\zeta\mathrm{l}}$. As the iso-damping contour $C_{\zeta\mathrm{l}}$ is open, the boundary $B_{\zeta\mathrm{l}}(\omega_i)$ is finally closed by connecting the two extreme points obtained.

Figure 19 shows that the critical point $(-\pi,$ 0 dB) can be outside the area defined by this boundary. This does not really matter as the composite boundary $B_0(\omega_i)$ finally used in QFT design is defined from the most restrictive parts of the set of boundaries. Indeed other boundaries defined from

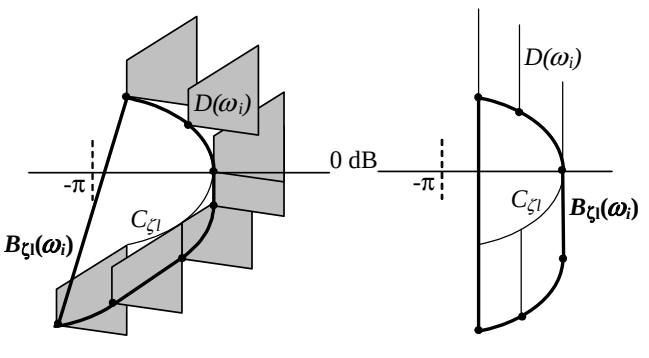

(a) (b)

Fig. 19. Construction of $B_{\zeta\mathrm{l}}$ boundaries for QFT designs for two types of uncertainty domains $D(\omega_i)$: (a) polygonal shape; (b) rectilinear shape.

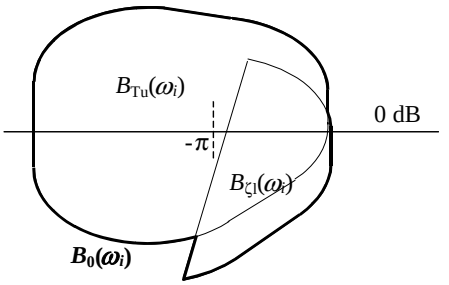

Fig. 20. Construction of a B_0 composite boundary for QFT design.

M_{Tu} and M_{Su} ensure that the critical point is not approached. Figure 20 presents the construction of a composite boundary from peak magnitude and damping boundaries.

6. Conclusion

This paper showed that the two poles of the stable closed loop transfer function $\beta(s)/(1+\beta(s))$ with $\beta(s)$ defined by (4) tends to the right half-plane conjugated poles of the unstable transfer function $\beta(s)/(1+\beta(s))$ with $\beta(s)$ defined by (1). Thus, these right half-plane poles can be taken into account as the dominant poles of a closed loop defined from a lightly band-limited complex order integrator, and can be used to build iso-damping contours. Then three control design methodologies have been presented to show how these contours can be used to obtain robust controllers (PID, CRONE and QFT).

References

Åström, K. J. [1999] "Model uncertainty and robust control design," *Cosy Workshop — ESF Course* (Valencia, Spain).

Banos, A., Cervera, J., Lanusse, P. & Sabatier, J. [2008] "Bode optimal loop shaping with CRONE compensators," *Proc. 14th IEEE Mediterranean Electrotechnical Conf.*, pp. 48–53.

Bode, H. W. [1945] *Network Analysis and Feedback Amplifier Design* (Van Nostrand, NY).

Cervera, J. & Banos, A. [2008] "Automatic loop shaping in QFT using CRONE structures," *J. Vib. Contr.* **14**, 1375–1388.

D'Azzo, J. J. & Houpis, C. H. [1995] *Linear Control System Analysis and Design, Conventional and Modern* (McGraw Hill Publishing Co., NY).

Horowitz, I. M. & Sidi, M. [1972] "Synthesis of feedback systems with large plant ignorance for prescribed time-domain tolerances," *Int. J. Contr.* **16**, 287–309.

Horowitz, I. M. [1991] "Survey of quantitative feedback theory (QFT)," *Int. J. Contr.* **53**, 255–291.

Horowitz, I. M. [1993] *Quantitative Feedback Design Theory — QFT* (QFT Publications, Boulder, Colorado).

Lanusse, P., Oustaloup, A., Ceyral, C. & Nouillant, M. [1992] "Optimal CRONE control of a tractor hich system," *Nonlinear Control System Design Symp.* (*NOLCOS'92*) (Bordeaux, France).

Lanusse, P., Oustaloup, A. & Mathieu, B. [1993] "Third generation CRONE control," *IEEE/SMC'93 Conf.* (Le Touquet, France).

Lanusse, P. [1994] *De la Commande CRONE de Première Génération à la Commande CRONE de Troisième Generation*, PhD thesis, Bordeaux I University, France.

Lanusse, P., Oustaloup, A. & Sutter, D. [1996] "Multiscalar CRONE control of multivariable plants," *WAC'96 — ISIAC Symphosia* (Montpellier, France).

Lanusse, P., Oustaloup, A. & Mathieu, B. [2000] "Robust control of LTI square MIMO plants using two CRONE control design approaches," *IFAC Symp. Robust Control Design "ROCOND 2000"* (Prague, Czech Republic).

Lanusse, P. & Oustaloup, A. [2006] "Study of fractional Wiener/Hammerstein systems in closed-loop," *2nd IFAC Workshop on Fractional Differentiation and Its Applications* (*FDA'06*) (Porto, Portugal).

Nelson-Gruel, D., Lanusse, P. & Oustaloup, A. [2008] "Decentralized CRONE control of mxn multivariable system with time-delay," *3nd IFAC Workshop on "Fractional Differentiation and Its Applications"* (*FDA'08*) (Ankara, Turkey).

Nelson-Gruel, D., Lanusse, P. & Oustaloup, A. [2009] "Robust control design for multivariable plants with time-delays," *Chem. Eng. J.* **146**, 414–427.

Oustaloup, A. [1983] *Systèmes Asservis Linéaires d'ordre Fractionnaire* (Masson, Paris).

Oustaloup, A. [1991] *La Commande CRONE* (Hermes Editor, Paris).

Oustaloup, A., Mathieu, B. & Lanusse, P. [1995a] "Integration non entière complexe et contours d'iso-amortissement," *RAIRO-APII* **29**, 177–203 (Ed. Hermes, Paris).

Oustaloup, A. & Mathieu, B. [1995b] "Robust control of SISO plants: The CRONE control," *ECC'95* (Rome, Italia).

Oustaloup, A., Lanusse, P. & Mathieu, B. [1995c] "The CRONE control of resonant plants: Application to a flexible transmission," *Eur. J. Contr.* **1**, 113–121.

Oustaloup, A., Levron, F., Nanot, F. & Mathieu, B. [2000] "Frequency band complex non-integer differentiator: Characterization and synthesis," *IEEE Trans. Circuit Syst.* **47**, 25–40.

Oustaloup, A., Pommier, V. & Lanusse, P. [2003] "Design of a fractional control using performance contours — Application to an electromechanical system, *Fract. Cal. Appl. Anal.* **6**, 1–24.

Pommier, V., Sabatier, J., Lanusse, P. & Oustaloup, A. [2002] "CRONE control of a nonlinear hydraulic actuator," *Contr. Eng. Pract.* **10**, 391–402.

Pommier-Budinger, V., Lanusse, P., Janat, Y. & Oustaloup, A. [2005] "CRONE control of MIMO plants," *ECC-CDC 05* (Seville, Spain).

Pommier-Budinger, V., Lanusse, P., Sabatier, J. & Oustaloup, A. [2006] "Fractional robust control of a nonlinear plant: Control of a nonlinear testing bench using the singular perturbation technique and the CRONE approach," *J. Européen des Systèmes Automatisés* (*JESA*) **40**, 211–232.

Pommier-Budinger, V., Janat, Y., Nelson-Gruel, D., Lanusse, P. & Oustaloup, A. [2008] "Fractional robust control with iso-damping property," *American Control Conf. 2008* (Seattle, WA, June 11–13, 2008).

Sabatier, J., Oustaloup, A., Garcia Iturricha, A. & Lanusse, P. [2002] "CRONE control: Principles and extension to time varying systems with asymptotically constant coefficients," *Nonlin. Dyn.* **29**, 363–385.